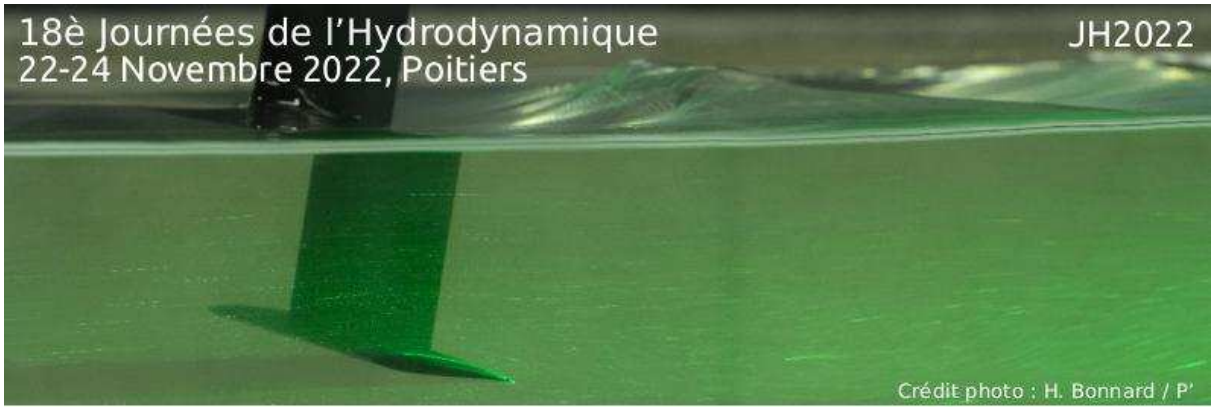

WAVE LOADS ON A GRAVITY BASE STRUCTURE SITTING ON A GRAVEL BED

EFFORTS DE HOULE SUR UNE GBS ASSISE SUR UN LIT POREUX

B. MOLIN[(1)], A. CINELLO[(2)], A. MARTY[(2)], B. THIBAULT[(2)]

bmolin@centrale-marseille.fr; acinello@oceanide.net; amarty@oceanide.net; bthibault@oceanide.net

[(1)] Aix Marseille Univ, CNRS, Centrale Marseille, IRPHE UMR7342, Marseille

[(2)] Océanide, BP 63, 83502 La Seyne sur Mer cedex

Abstract

The topic of this paper is the prediction of the wave loads upon Gravity Base Structures (GBS) sitting on gravel beds. A numerical model is first described, based on linearized potential flow theory. This model assumes a simplified geometry consisting in two superimposed truncated cylinders. Experiments are carried out in the 'South France - Ocean Basin', in regular waves, with different types of gravel beds. Measured pressures (inside the gravel beds) and loads are compared with the numerical predictions.

Résumé

L'étude présentée concerne la prédiction des efforts de houle sur des plateformes de type GBS (Gravity Base Structure) supportées par des lits poreux (enrochements). Un modèle numérique est développé, basé sur la théorie potentielle linéarisée, pour une géométrie simplifiée : un cylindre vertical porté par une embase cylindrique également circulaire. Des essais sont réalisés dans le bassin de génie océanique 'South France - Ocean Basin', pour différents types de lits poreux. Pressions et efforts, calculés et mesurés, sont comparés.

Introduction

Gravity Base Structures (GBS) are alternative supports for offhore wind turbines, in intermediate waterdepths. For instance the Fécamp wind farm consists in 71 GBS supported turbines (see Figure 1) in 25-30 meters depths. When installed these GBS are usually sitting on gravel beds (Esteban et al., 2015). As the waves pass by, some effects are felt within the gravel bed, i.e. some flow and oscillatory wave induced pressures, that contribute to the wave loading.

FIGURE 1 – Fécamp wind farm GBS under construction. Bouygues Travaux Publics. © Jacques Basile.

This is the problem considered here, through numerical and experimental modelling. The numerical model is based on linearized potential flow theory. The flow and induced pressures in the gravel bed are modeled following the theory of Sollitt & Cross (1972). For the sake of simplicity the geometry of the GBS consists in two superimposed circular cylinders (Figure 2).

Section 1 describes the theoretical model where, thanks to the simple geometry, the matched eigen-function expansion method is applied in its resolution. Section 2 describes the experiments carried out in the 'South France - Ocean Basin', and presents some comparisons between measurements and calculations. Finally an Appendix describes sloshing tests performed to determine the inertia and friction coefficients of the various materials used to model the gravel bed.

I – Theory

I – 1 General equations

Application is made of linearized potential flow theory. The flow through the gravel bed is modeled following the theoretical model of Sollitt & Cross (1972), widely applied in coastal engineering, the main application there being the performance of permeable breakwaters. In this model the flow through the porous medium is also assumed to be irrotational and described by linearized potential flow theory. Compared to the clear water flow, additional inertia and dissipative terms are introduced in the Bernoulli equation, which becomes

$$p = p_0 - \rho g\, z - \rho\, S\, \frac{\partial \Phi}{\partial t} + \mathrm{i}\ \rho\, \omega\, f\, \Phi \tag{1}$$

where the velocity potential Φ is periodic at the wave frequency ω :

$$\Phi(x, y, z, t) = \Re\left\{\varphi(x, y, z)\, \mathrm{e}^{-\mathrm{i}\ \omega\, t}\right\} \tag{2}$$

The inertia coefficient S is usually related to an added mass coefficient C_a of the constituants of the porous medium, through

$$S = 1 + \frac{1 - \epsilon}{\epsilon}\, C_a \tag{3}$$

where ϵ is the porosity of the porous medium (volume occupied by water divided by total volume). f is a friction coefficient, to be determined.

The matching conditions at the boundaries between clear water (1) and porous medium (2) are :

1. Mass conservation

$$\nabla\varphi_1 \cdot \overrightarrow{n} = \epsilon\, \nabla\varphi_2 \cdot \overrightarrow{n} \tag{4}$$

2. Equality of the dynamic pressures

$$\varphi_1 = (S + \mathrm{i}\ f)\, \varphi_2 \tag{5}$$

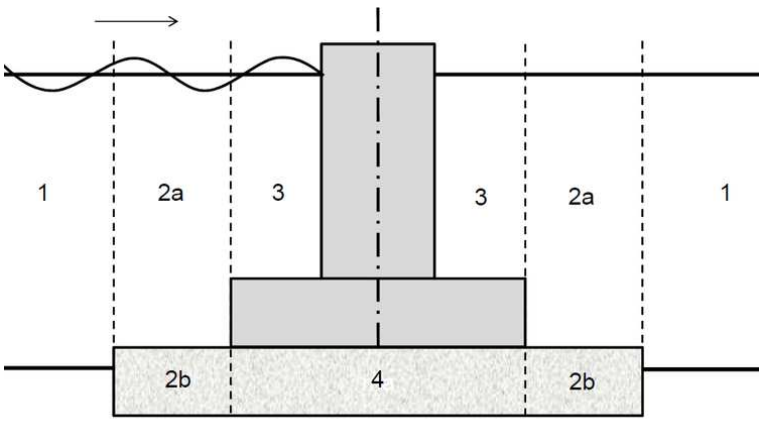

FIGURE 2 – Geometry. Annular domains.

The potential φ is the solution of the following boundary value problem :

$$\begin{aligned}
\Delta\varphi &= 0 && \text{in the fluid domain} && (6)\\
g\,\varphi_z - \omega^2\,\varphi &= 0 && z = 0 \ \text{(free surface)} && (7)\\
\varphi_n &= 0 && \text{on the body surface and sea floor} && (8)\\
\mathrm{Rad}\,(\varphi - \varphi_I) & && x^2 + y^2 = R^2 \to \infty && (9)
\end{aligned}$$

where the last condition means that the diffracted potential $\varphi_D = \varphi - \varphi_I$ (φ_I being the potential of the incoming waves) satisfies a radiation condition at infinity (radially outgoing waves of amplitude decaying as $R^{-1/2}$).

Advantage is first taken of the vertical axisymmetry to decompose the potential as a Fourier series with respect to the azimutal angle θ :

$$\varphi(R, z, \theta) = \sum_{m=0}^{\infty} \varphi_m(R, z)\ \cos m\theta \tag{10}$$

Then a matched eigenfunction expansion method is applied : the fluid domain (R, z) is decomposed into 4 annular subdomains 1 through 4, as shown in Figure 2. In each subdomain the potential φ_m is written as a sum of functions $F_{mn}(R)\, G_{mn}(z)$ which satisfy the Laplace equation (6), the free surface condition (30), and the no-flow condition at the sea floor and at the keel of the GBS. The unknown coefficients in the expansions are then determined by matching the potentials and their radial derivatives at the boundaries between the successive domains.

I – 2 Eigenfunction expansions

Figure 2 shows the 4 subdomains : the outer domain (1), from $R = c$ to infinity, where c is the radius of the gravel bed (see Figure 3) ; domain 2, annular, from $R = b$ to $R = c$, partly free water, partly gravel bed ; domain 3, above the base of the GBS ; and domain 4, below the GBS.

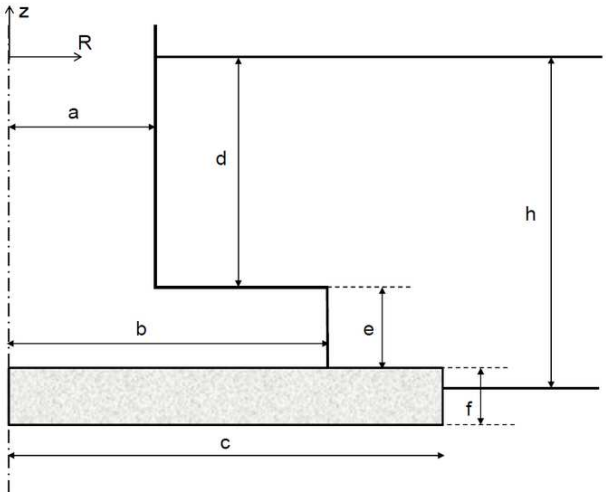

FIGURE 3 – Geometrical parameters.

Be $\Phi(R, z, \theta, t)$ the velocity potential, periodic in time at the wave frequency ω :

$$\Phi(R, z, \theta, t) = \Re\left\{-\mathrm{i}\,\frac{A\,g}{\omega}\,\varphi(R, z, \theta)\,\mathrm{e}^{-\mathrm{i}\,\omega t}\right\} \tag{11}$$

with A the wave amplitude and φ the "reduced potential". Regular incoming waves are propagating along the Ox axis, with the potential

$$\varphi_I = \frac{\cosh k_0(z+h)}{\cosh k_0 h}\,\mathrm{e}^{\mathrm{i}\,kR\cos\theta} = \frac{\cosh k_0(z+h)}{\cosh k_0 h}\,\sum_{m=0}^{\infty}\varepsilon_m\,\mathrm{i}^{\,m}\,J_m(k_0R)\,\cos m\theta = \sum_{m=0}^{\infty}\varphi_{Im}\,\cos m\theta \tag{12}$$

with k_0 the wave number linked to the frequency ω through the dispersion equation $\omega^2 = gk_0\,\tanh k_0 h$, and J_m the Bessel function of the first kind ($\varepsilon_m = 1$ for $m = 0$, $\varepsilon_m = 2$ otherwise).

In the 4 subdomains of Figure 2, the total velocity potential (incident plus diffracted) can be written as :

– Domain 1 : $R > c$ (exterior)

$$\varphi_{1m} = \varphi_{Im} + A_{m0}\,\frac{H_m(k_0R)}{H_m(k_0c)}\,\frac{\cosh k_0(z+h)}{\cosh k_0 h} + \sum_{n=1}^{\infty}A_{mn}\,\frac{K_m(k_nR)}{K_m(k_nc)}\,\cos k_n(z+h) \tag{13}$$

with k_0, k_n the roots of the dispersion equation

$$\omega^2 = gk_0\,\tanh k_0 h = -gk_n\,\tan k_n h \tag{14}$$

H_m the Hankel function $H_m = J_m + \mathrm{i}\,Y_m$, Y_m the Bessel function of the second kind, K_m the modified Bessel function of the second kind.

The z functions $[\cosh k_0(z+h),\ \cos k_n(z+h)]$ form a complete and orthogonal set over the interval $[-h\ 0]$.

– Domain 2 : $b < R < c$

$$\varphi_{2m} = \sum_{n=1}^{\infty} \left\{ B_{mn} \, \frac{J_m(\lambda_n R)}{J_m(\lambda_n c)} + C_{mn} \, \frac{H_m(\lambda_n R)}{H_m(\lambda_n b)} \right\} \, f_n(z) \tag{15}$$

where the λ_n are the roots of a complex dispersion equation that can be written in the form (Chang & Liou, 2006)

$$\Gamma - x \, \tanh \beta x - \Phi \, \tanh \alpha x \, (x - \Gamma \, \tanh \beta x) = 0 \tag{16}$$

with $\Gamma = \omega^2 H/g$, $\alpha = f/H$, $\beta = (d+e)/H$, $\Phi = \epsilon/(S + \mathrm{i}\, f)$, $H = d + e + f$ being the total height, S the inertia coefficient, f the friction coefficient.

The complex wave numbers λ_n are obtained by solving equation (16) with the homotopy method of Chang & Liou (2006). The z functions f_n in (15) are given by

- for $-H \leq z < -d - e$

$$f_n(z) = \alpha_n \, \cosh \lambda_n (z + H) \tag{17}$$

$$\alpha_n = \frac{\lambda_n \, \cosh \lambda_n (d+e) - \omega^2/g \, \sinh \lambda_n (d+e)}{(S + \mathrm{i}\, f) \, \lambda_n \, \cosh \lambda_n f} \tag{18}$$

- for $-d - e < z \leq 0$

$$f_n(z) = \cosh \lambda_n z + \frac{\omega^2}{g \, \lambda_n} \, \sinh \lambda_n z \tag{19}$$

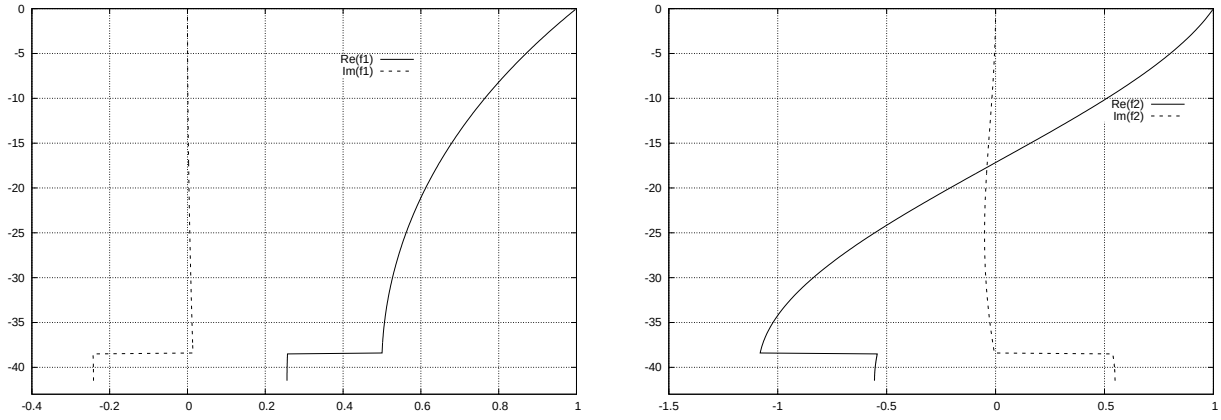

FIGURE 4 – Functions $f_1(z)$ and $f_2(z)$.

The f_n functions are discontinuous in value and in slope at the boundary between the water and the gravel bed (see Figure 4). They are orthogonal over the whole height $-H \leq z \leq 0$ with the following norm :

$$\int_{-H}^{0} \chi(z) \, f_m(z) \, f_n(z) \, \mathrm{d}z \equiv 0 \tag{20}$$

for $m \neq n$, with $\chi(z) = \epsilon \, (S + \mathrm{i}\, f)$ below the interface, $\chi(z) = 1$ above.

– Domain 3 ($a \leq R \leq b$)

$$\begin{aligned} \varphi_{3m} &= D_{m0} \, \frac{Y'_m(\mu_0 a) \, J_m(\mu_0 R) - J'_m(\mu_0 a) \, Y_m(\mu_0 R)}{Y'_m(\mu_0 a) \, J_m(\mu_0 b) - J'_m(\mu_0 a) \, Y_m(\mu_0 b)} \, \frac{\cosh \mu_0 (z+d)}{\cosh \mu_0 d} \\ &+ \sum_{n=1}^{\infty} D_{mn} \, \frac{I'_m(\mu_n a) \, K_m(\mu_n R) - K'_m(\mu_n a) \, I_m(\mu_n R)}{I'_m(\mu_n a) \, K_m(\mu_n b) - K'_m(\mu_n a) \, I_m(\mu_n b)} \, \cos \mu_n (z+d) \end{aligned} \tag{21}$$

with μ_0, μ_n the roots of the dispersion equation in a water depth equal to d :

$$\omega^2 = g\mu_0 \tanh \mu_0 d = -g\mu_n \tan \mu_n d \tag{22}$$

The no-flow conditions in $z = -d$ and in $R = a$ are satisfied a priori by (21).

– Domain 4 (part of the gravel bed below the GBS)

$$\varphi_{4m} = E_{m0} \left(\frac{R}{b}\right)^m + \sum_{n=1}^{\infty} E_{mn} \frac{I_m(\nu_n R)}{I_m(\nu_n b)} \cos \nu_n (z + H) \tag{23}$$

where $\nu_n = n\,\pi/f$ and $H = d + e + f$.

In equations (21) and (23), again, the functions I and K are the modified Bessel functions.

The unknown coefficients $A_{mn}, \ldots, E_{mn}$ are obtained by matching the values of the velocity potentials and of their radial derivatives at the common boundaries. This holds for water to water interface. At the boundaries between water and gravel bed (that is for $R = c$, $-h \leq z \leq -d-d$), equations (4) and (5) are used.

I – 3 Matching

Advantage is taken of the orthogonality of the z functions over their respective domains to ensure the matching. Because of lack of space details are not given. The series (13), (15), (21) and (23) are truncated at finite orders N_1, N_2, N_3 and N_4. The A_{mn}, D_{mn} and E_{mn} coefficients are first eliminated, to end up with a linear problem in (B_{mn}, C_{mn}), of rank $2N_2$, solved by a Gauss method.

The hydrodynamic loads can then be computed, integrating (analytically) the pressure $p =$ i $\rho\,\omega\,\varphi$ on the GBS. In the gravel bed the pressure i $\rho\,\omega\,(S +$ i $f)\,\varphi$ is integrated on a corrected GBS surface, accounting for a surfacic porosity τ taken to be equal to $1 - (1 - \epsilon)^{2/3}$ (assuming isotropic volumic porosity). This means that a factor τ is further applied to the pressure before integration. The $m = 0$ coefficients contribute to the vertical load, while the $m = 1$ coefficients yield the horizontal load and overturning moment. Higher m values do not contribute to the global loads, but they do to the local pressures.

II – Experimental campaign

The tests are done in the 'South France - Ocean Basin', at a scale 1 : 30. Figure 5 shows the full scale dimensions of the GBS. The waterdepth is 40 m. The tests are run in regular waves, with (full scale) periods ranging from 8 to 16 seconds and heights up to 11.5 meters. Two wave heights are produced at each wave period. Based on the column diameter (9.45 m), the maximum K_C numbers are less than 5, implying that the flow should be close to fully attached in all tests.

Material	Porosity	Size	Density (kg/m^3)	f
Small rocks (M1)	0.41	3 to 6 mm	2680	4.5
PVC pellets (M2)	0.38	4 mm (D) × 2 mm (h)	1400	6.0
Glass balls (M3)	0.39	10 mm (D)	2510	2.4
Foam (M4)	0.9		17	10.0

The tests are run without gravel bed (with the GBS slightly above the tank floor), and with 4 different types of porous media, described in the Table (see also Figure 6). In the Table are also shown the friction coefficients f, as determined through the sloshing tests reported in the Appendix. As explained there, it was not possible, from these tests, to derive precise values of

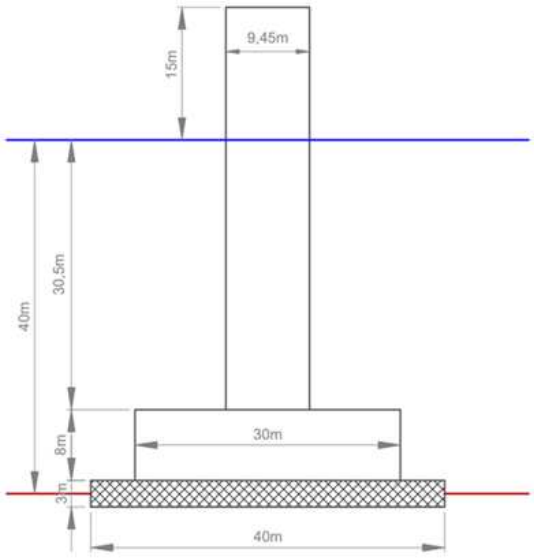

FIGURE 5 – GBS dimensions.

FIGURE 6 – Granular media : small rocks (case 1), PVC pellets (case 2), glass balls (case 3), foam (case 4).

the inertia coefficient S, which seems to be very small for all media. As will be seen further its value has a very small impact on the predicted loads and pressures.

The part of the gravel bed (in cases 1, 2, 3) outside the bottom of the GBS is covered by a wire net (Figure 7) to avoid scouring.

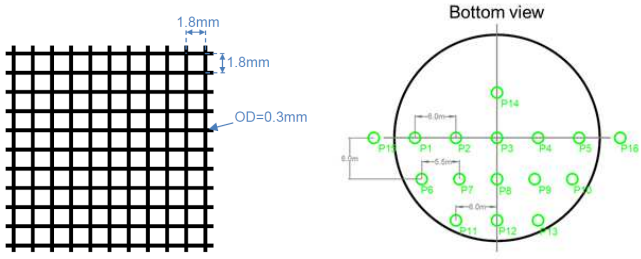

FIGURE 7 – Wire net geometry and locations of the pressure sensors.

The GBS model is mounted on four 3D load cells that deliver the wave loads (F_x and F_z) and the overturning moment M_y. Fourteen pressure sensors are inserted within the bottom of the GBS and two additional ones (P15 and P16) are located within the gravel bed (Figure 7).

Before proceeding to comparisons with experimental measurements, the numerical model was duely validated, and run extensively to investigate the sensitivity of the wave loads and pressures to the porosity and hydrodynamic parameters (inertia and friction coefficients) of the

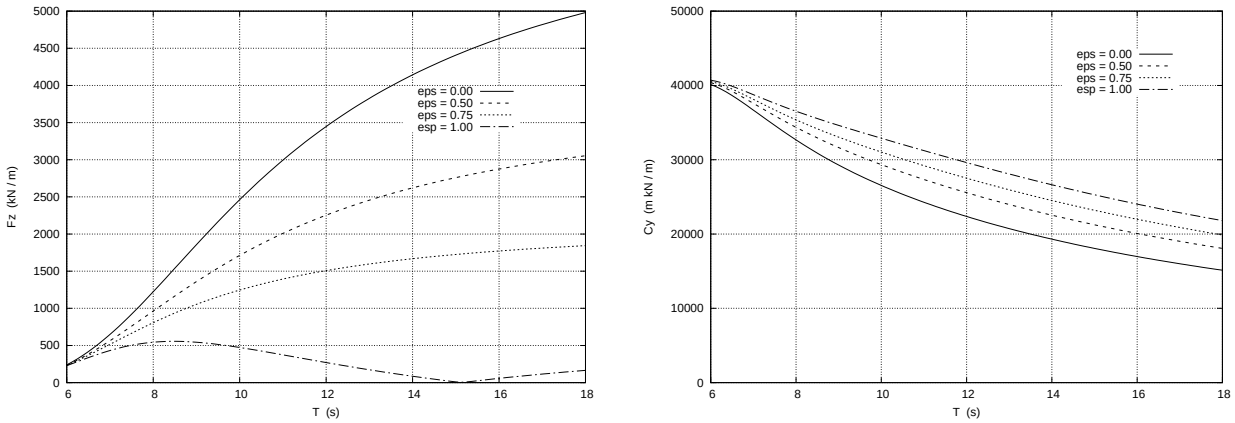

FIGURE 8 – Calculated vertical load (left) and overturning moment (right). Effect of varying the porosity.

gravel bed. Somewhat disappointingly it was found that the pressures were nearly insensitive to all parameters. As for the loads a strong sensitivity to the porosity was observed (see Figure 8), associated with the τ coefficient applied to the pressure before integration on the hull. As written earlier τ is the surfacic porosity, based on the assumption of isotropic volumic porosity ($\tau = 1 - (1 - \epsilon)^{2/3}$). Not much information seems to be available in literature on the matter. Intuitively the compactness and the weight in water of the gravel bed may play some role.

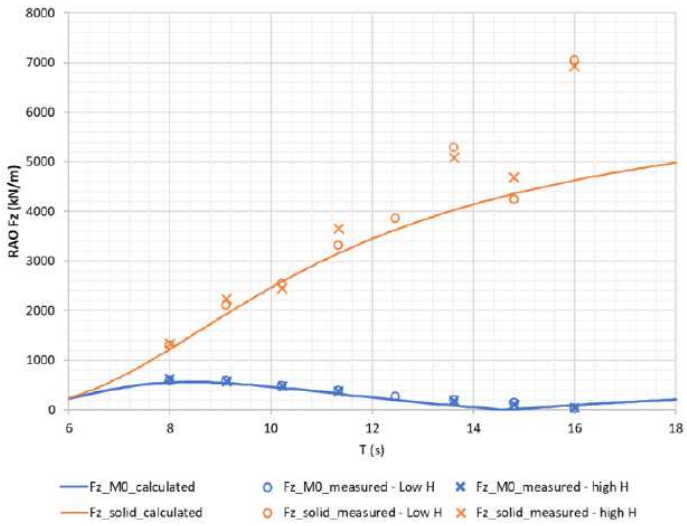

FIGURE 9 – Measured and calculated vertical load. Solid and fully drained cases.

Figure 9 shows the measured and calculated RAOs of the vertical load, in the fully drained (M0) and undrained cases. Fully drained means with no gravel bed. The undrained load was obtained by subtracting the integrated pressures measured at the bottom. It is not really equivalent to the solid gravel bed case since the flows above the GBS base may slightly differ. It can be seen that the agreement between calculated and measured loads is quite good in the M0 case. In the solid case there is some scatter at the highest wave periods. This is partly due to reflections taking place at the end of the false bottom and lower efficiency of the attenuation beach at large wave periods.

Figure 10 shows the same comparisons for the overturning moment, with fair agreement between calculations and measurements.

Finally Figure 11 shows, for the 4 gravel beds tested, the RAOs of the measured and calculated pressures at the gauge P3, at the center of the GBS bottom. As already written the

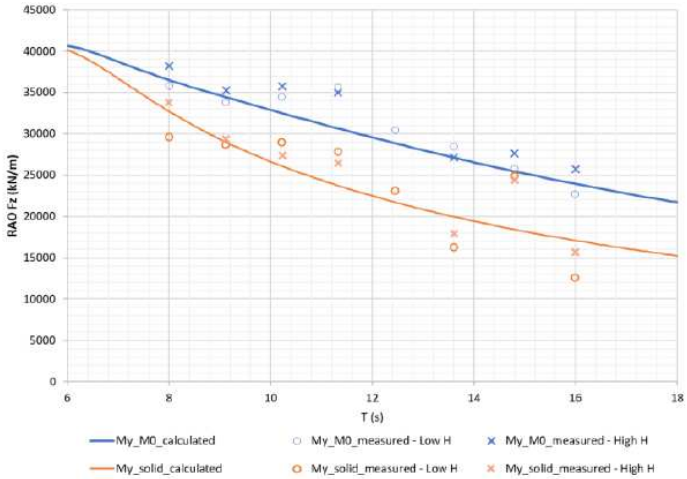

FIGURE 10 – Measured and calculated overturning moment. Solid and fully drained cases.

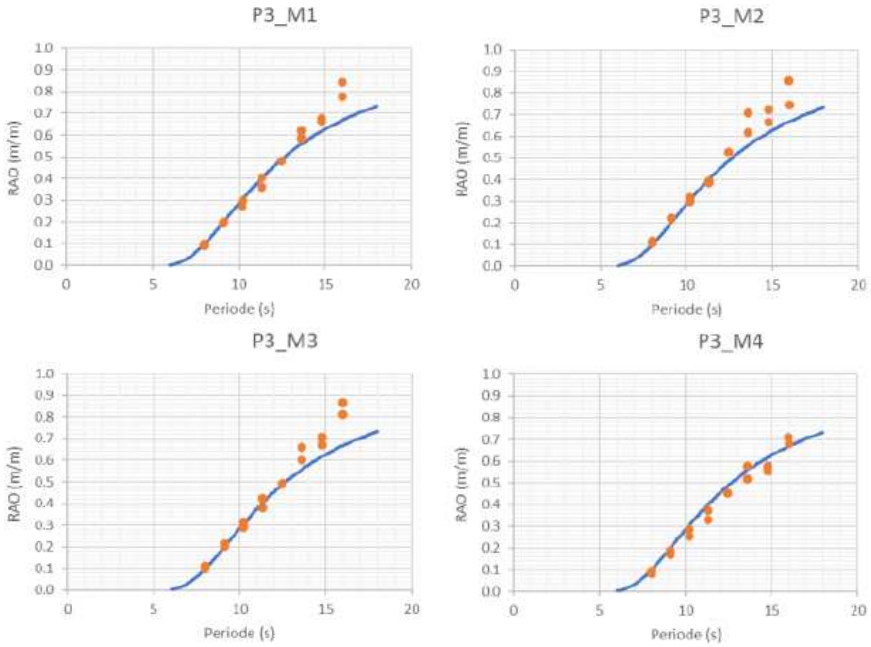

FIGURE 11 – Measured and calculated pressures in the 4 gravel bed cases.

numerical model gave quasi identical pressures for all media. This is confirmed by the measurements which also gave nearly equal values. The agreement between measured and claculated pressures is rather good except at the highest wave periods where there is some scatter in the experimental values, generally lying above the calculated ones. As written earlier, this is probably associated with the reflections taking place from the end of the false bottom and from the beach, not allowing for a sufficient time for a steady state to take place.

Unfortunately the loads measured by the force sensors turned out to be unreliable, in total disagreement with the values derived from the pressure sensors. For solid media, and as expected, the measurements from the load cells were affected by the fact that a part of the load goes through the media itself. For the foam case, it is presumed that the pressure exerted by the GBS on the foam has affected its physical properties and notably its surface porosity that plays an important role on the resulting vertical load and overturning moment.

III – Summary

This work presents the results of a numerical model developed to predict the wave loads upon GBS sitting on gravel beds. The numerical model is compared to experimental results obtained during a test campaign carried out in the 'South France - Ocean Basin' operated by Océanide where different porous media under the GBS are tested. The comparison of measured pressures below the GBS shows a good agreement with the calculated pressures from the developed numerical model.

Numerical model and experiments show very close pressures for all considered media. It was found that pressures were quasi-insensitive to the media hydrodynamic properties and that the differences seen on the vertical load and overturning moment were mainly driven by the media surface porosity applied to the pressure before integration.

Finally, the different tested media were characterized using an experimental method based on sloshing tests performed with an Hexapod with the objective of establishing their hydrodynamic properties (friction and added mass coefficient). Results extracted from this experimental procedure lead to the conclusion that it is a very effective way to characterize the hydrodynamic properties of a porous medium.

Acknowledgements

This project was financed through the CITEPH 2022 program by Doris Engineering, SAIPEM S.A. and TotalEnergies One Tech. The authors are grateful to the sponsors for permission to publish.

Appendix

Sloshing tests are performed with an Hexapode set-up : a rectangular tank, partly filled with granular media and water, is subjected to forced horizontal motion. From the amplitude of the sloshing response, the hydrodynamic characteristics of the granular media are obtained. The tank is 1.17 m long and 0.277 m wide (internal dimensions). The height of the gravel bed is 0.15 m in all tests. Three different cases of water heights are considered : 0.25 m, 0.30 m (only in the glass ball case), and 0.35 m. (These values are the total heights, gravel bed plus water layer above.)

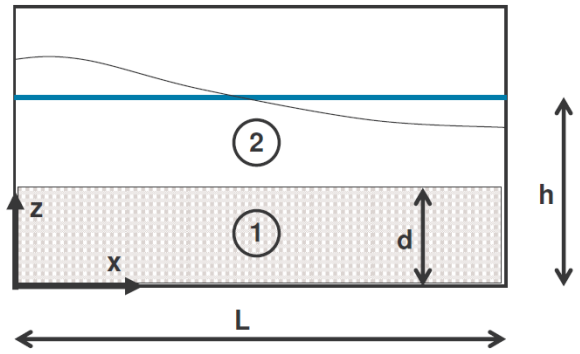

FIGURE 12 – Geometry.

The tank motion is sinusoidal along the Ox axis, with amplitude A and frequency ω :

$$X(t) = A \sin \omega t \tag{24}$$

A steady state is assumed to have been reached, so that all physical quantities are periodic in time at frequency ω :

$$\Phi(x, z, t) = \Re \left\{ A\,\omega\, \varphi(x, z)\, \mathrm{e}^{-\mathrm{i}\,\omega t} \right\} \tag{25}$$

The tank is divided into two subdomains, the gravel bed (subdomain 1) and the water layer above (subdomain 2). In each subdomain, the velocity potential φ_i verifies the Laplace equation.

The potentials φ_1 and φ_2 are written as

$$\varphi_1 = x - \frac{L}{2} + \sum_{n=1}^{\infty} A_n \frac{\cosh \lambda_n z}{\cosh \lambda_n d} \cos \lambda_n x \tag{26}$$

$$\varphi_2 = x - \frac{L}{2} + \sum_{n=1}^{\infty} (B_n \cosh \lambda_n (z-d) + C_n \sinh \lambda_n (z-d)) \cos \lambda_n x \tag{27}$$

with $\lambda_n = n\,\pi/L$, L the tength of the tank, d the height of the gravel bed, h the total height from the tank floor up to the still free surface (see Figure 12). Under this form φ_1 and φ_2 verify the Laplace equation and the no-flow condition at the solid boundaries.

Projecting $x - L/2$ on the set $[\cos \lambda_n x]$, one obtains

$$\varphi_1 = \sum_{n=1}^{\infty} \left[A_n \frac{\cosh \lambda_n z}{\cosh \lambda_n d} + \alpha_n \right] \cos \lambda_n x \tag{28}$$

$$\varphi_2 = \sum_{n=1}^{\infty} [B_n \cosh \lambda_n (z-d) + C_n \sinh \lambda_n (z-d) + \alpha_n] \cos \lambda_n x \tag{29}$$

where $\alpha_n = -4\,L/(n^2\pi^2)$ for n odd and $\alpha_n = 0$ for n even.

The remaining boundary conditions to satisfy are :

• The free surface condition :

$$g\,\varphi_{2z} - \omega^2\,\varphi_2 = 0 \qquad z = h \tag{30}$$

• The mass conservation at the boundary between the two domains :

$$\varphi_{2z} = \epsilon\,\varphi_{1z} \qquad z = d \tag{31}$$

• The equality of the pressures :

$$\varphi_2 = (S + \mathrm{i}\ f)\varphi_1 \qquad z = d \tag{32}$$

At each order n the following linear system is obtained :

$$\begin{pmatrix} S + \mathrm{i}\ f & -1 & 0 \\ \epsilon \tanh \lambda_n d & 0 & -1 \\ 0 & g\lambda_n \tanh \lambda_n (h-d) - \omega^2 & g\lambda_n - \omega^2 \tanh \lambda_n (h-d) \end{pmatrix} \begin{pmatrix} A_n \\ B_n \\ C_n \end{pmatrix} = \alpha_n \begin{pmatrix} 1 - S - \mathrm{i}\ f \\ 0 \\ \omega^2 \cosh^{-1} \lambda_n (h-d) \end{pmatrix} \tag{33}$$

When this is solved the RAO of the free surface motion at the wall (in $x = 0$) is obtained as :

$$\mathrm{RAO}_\eta = \frac{\mathrm{i}\ \omega^2}{g} \left[\sum_{n\ \mathrm{impair}} B_n \cosh \lambda_n (h-d) + C_n \sinh \lambda_n (h-d) + \alpha_n \right] \tag{34}$$

Due to lack of space, we present only two figures. Figure 13 shows purely numerical results, in the 25 cm waterheight case, with a porosity equal to 40 %, where the added mass coefficient is set to zero and the friction coefficient (f in the figure) is varied. There is an f value where the RAO goes through a minimum (where viscous dissipation is maximized). The peak sloshing frequency also appears to be quite sensitive to the f value. As the C_a coefficient is increased from zero, the minimum peak RAO value increases and the frequency range shrinks. In all cases it was found that the otimum C_a value had to be taken very close to zero. Figure 14 shows the experimental and numerical RAOs obtained with the glass balls, with a rather good agreement. The same experimental points are obtained at 2 mm and 4 mm excitation amplitude, proving that nonlinear effects are negligible.

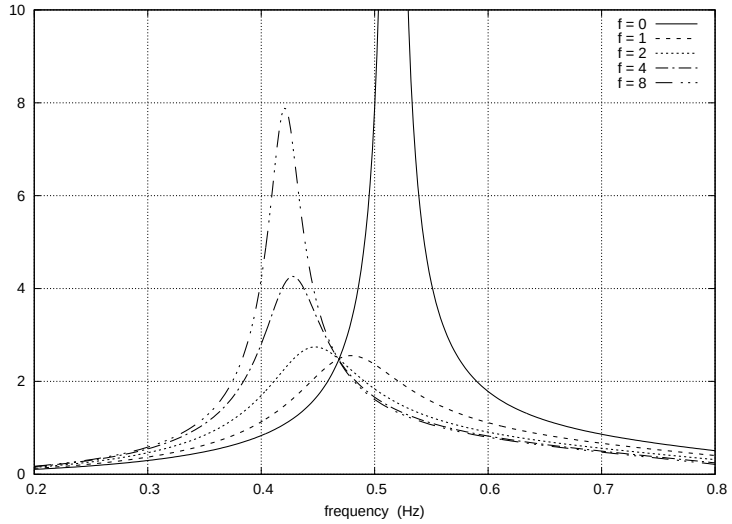

FIGURE 13 – Numerical RAOs of the free surface elevation. $\epsilon = 0.4$; $C_a = 0.0$; $h = 0.25$ m. Variable friction coefficient.

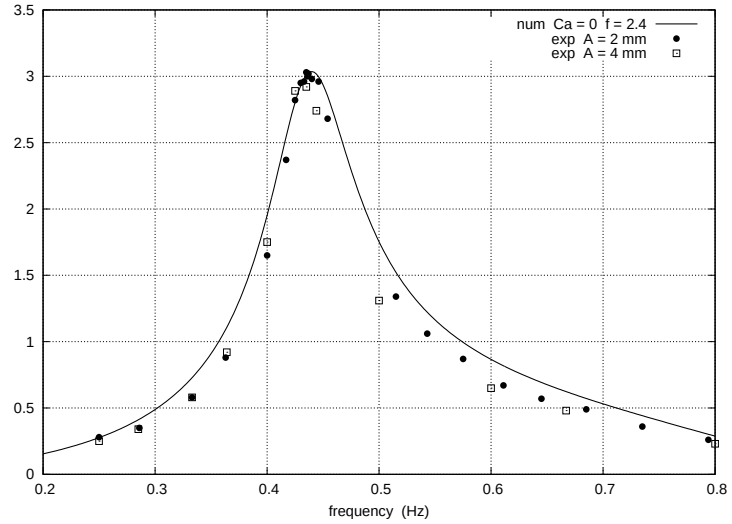

FIGURE 14 – Glass balls. Experimental and numerical RAOs of the free surface elevation.

References

CHANG H.K., LIOU J.C. 2006 Solving wave dispersion equation for dissipative media using homotopy perturbation technique, *J. Waterway, Port, Coastal and Ocean Engineering*, 132, 28-35.
ESTEBAN M.D., COUÑAGO B., LÓPEZ-GUTIÉRREZ J.S., NEGRO V., VELLISCO F. 2015 Gravity based support structures for offshore wind turbine generators : Review of the installation process, *Ocean Eng.*, **110**, 281-291.
SOLLITT C.K. & CROSS R.H. 1972 Wave transmission through permeable breakwaters, *Proc. 13th Int. Conf. on Coastal Engineering*, ASCE, 1827-1846.